CrystEngComm

PAPER

Cite this: *CrystEngComm*, 2018, **20**, 2608

General strategy for lanthanide coordination polymers constructed from 1,1′-ferrocenedicarboxylic acid under hydrothermal conditions†

Xue-Dong Du,[a] Weiwei Zheng,[b] Xiao-Hong Yi,[a] Jiong-Peng Zhao,*[c] Peng Wang[a] and Chong-Chen Wang *[a]

Twenty-six lanthanide coordination polymers (CPs), $Ln_2(fcd)_2(phen)_2(NO_3)_2$ (Ln = Nd (**1-Nd**)), $[Ln_2(fcd)_3(phen)_2]\cdot(CH_3OH)_2$ (Ln = Sm (**2-Sm**), Eu (**2-Eu**), Gd (**2-Gd**), and Tb (**2-Tb**)), $Ln_2(fcd)_2(Hfcd)_2(phen)_2$ (Ln = La (**3-La**), Ce (**3-Ce**), Pr (**3-Pr**), Nd (**3-Nd**), Sm (**3-Sm**), and Gd (**3-Gd**)), $[Ln_2(fcd)_3(CH_3CH_2OH)_2(H_2O)_2]\cdot H_2O$ (Ln = La (**4-La**), Ce (**4-Ce**), Pr (**4-Pr**), Nd (**4-Nd**), Sm (**4-Sm**), Eu (**4-Eu**), Gd (**4-Gd**), Tb (**4-Tb**), Dy (**4-Dy**), Er (**4-Er**), Tm (**4-Tm**) and Yb (**4-Yb**)), and $[Ln_4(fcd)_6(H_2O)_2]\cdot nCH_3CH_2OH$ (Ln = Sm (**5-Sm**), Eu (**5-Eu**) and Tb (**5-Tb**)), were obtained from the reaction between 1,1′-ferrocenedicarboxylic acid (H_2fcd), 1,10-phenanthroline (phen) and the corresponding lanthanide salts under hydrothermal conditions. $Ln_2(fcd)_2(phen)_2(NO_3)_2$ (**1-Nd**) was constructed from discrete and neutral 0D dimeric units; $[Ln_2(fcd)_3(phen)_2]\cdot(CH_3OH)_2$ (**2-Sm/Eu/Gd/Tb**) and $Ln_2(fcd)_2(Hfcd)_2(phen)_2$ (**3-La/Ce/Pr/Nd/Sm/Gd**) were built up of 1D infinite chains, while $[Ln_2(fcd)_3(CH_3CH_2OH)_2(H_2O)_2]\cdot H_2O$ (**4-La/Ce/Pr/Nd/Sm/Eu/Gd/Tb/Dy/Er/Tm/Yb**) and $[Ln_4(fcd)_6(H_2O)_2]\cdot nCH_3CH_2OH$ (**5-Sm**, n = 0.33; **5-Eu**, n = 0.31; **5-Tb**, n = 0.30) were made up of 2D sheets. The different structures of these twenty-six CPs can be attributed to the variable conformations of fcd resulting from different reaction conditions like different counterions, ancillary ligands, temperatures, and solvents. Furthermore, the photoluminescence and magnetic properties of selected CPs have been characterized and discussed.

Received 11th February 2018,
Accepted 10th April 2018

DOI: 10.1039/c8ce00233a

rsc.li/crystengcomm

Introduction

Coordination polymers (CPs), as one of the favorite crystalline porous materials, have witnessed unprecedented rapid development in diverse areas[1–4] because of their compositional and geometric tenability,[5] ultrahigh surface area,[6] and multiple active sites.[2] Therefore, CPs have various potential applications on gas adsorption & separation,[7,8] catalysis,[2,9] luminescence,[10] and so on.[11,12] It is known that the crystallization, structure and morphology of CPs depend on the modulus of building blocks,[13] along with reaction conditions such as solvent,[14–16] the pH value of the reaction mixture,[17–19] temperature,[15,20] reaction & crystallization time,[21] the molar ratio & concentration of starting materials,[22–24] counterions,[25,26] auxiliary ligands,[27,28] and reaction pressure.[29] These parameters significantly influence the structural chemistry of organic ligands and the assembly of ligands with metal centers, which can finally lead to diverse and facilitating structures.

1,1′-Ferrocenedicarboxylic acid (H_2fcd), as a versatile organic ligand, has attracted much interest in coordination chemistry and has been exploited as a multifunctional ligand to construct various CPs due to its size and the strong inductive effect of the ferrocene unit. Up to now, a wide variety of CPs containing ferrocene have been obtained since ferrocene-containing complexes may possess many potential applications in catalysis[30,31] and electrical[32] and magnetic materials.[33–35] Furthermore, CPs containing lanthanide metals are of great interest due to their unique physicochemical properties.[36] So far, many homobinuclear and heterobinuclear lanthanide CPs have been reported.[33,37] However, the influence of reaction conditions on forming CPs with different crystal structures between 1,1′-

[a] *Beijing Key Laboratory of Functional Materials for Building Structure and Environment Remediation, Beijing University of Civil Engineering and Architecture, Beijing 100044, P. R. China. E-mail: chongchenwang@126.com*
[b] *Department of Chemistry, Syracuse University, Syracuse, New York 13244, USA*
[c] *School of Chemistry and Chemical Engineering, Tianjin University of Technology, Tianjin 300384, P. R. China*

† Electronic supplementary information (ESI) available: The details of synthesis, CHNO elemental data, FTIR data, crystallographic data, selected bond lengths and angles, and defined ring and relative parameters of the π–π interactions, crystallographic data in CIF. CCDC 1469569–1469581, 1469584, 1469585, 1469587–1469590 and 1568756–1568762. For ESI and crystallographic data in CIF or other electronic format see DOI: 10.1039/c8ce00233a

ferrocenedicarboxylic acid and lanthanide ions has not been explored. In this paper, twenty-six Ln-based CPs with zero-dimensional, one-dimensional, and two-dimensional structures were prepared *via* the reaction between various lanthanide ions and the H_2fcd ligand. The influences of different solvents, counterions, auxiliary ligands, and temperatures on tuning the formation were investigated. The magnetic and optical properties of selected CPs were also investigated.

Experimental

Materials and instruments

All reagents and solvents were purchased from J&K Scientific Ltd. and used directly without any further purification. CHNO elemental analyses were performed using an Elementar Vario EL-III instrument. Fourier transform infrared (FTIR) spectra were recorded with KBr pellets on a Nicolet 6700 spectrometer in the range of 4000–400 cm^{-1}. Fluorescence spectra were recorded on a Hitachi F-7000 spectrophotometer at room temperature. Both the excitation slit and the emission slit were set at 5 nm, and the acquisition time was 0.5 s. Magnetic susceptibilities were measured in the temperature range of 2–300 K under an applied magnetic field of 1000 Oe, and field dependent magnetization measurements were performed from 0 to 50 000 Oe at 2 K on a Quantum Design MPMS-XL-7SQUID magnetometer.

Synthesis of $Nd_2(fcd)_2(phen)_2(NO_3)_2$ (1-Nd). A mixture of $Nd(NO_3)_3{\cdot}6H_2O$ (0.6 mmol, 0.2629 g), 1,1′-ferrocenedicarboxylic acid (H_2fcd) (0.3 mmol, 0.0822 g) and 1,10-phenanthroline (phen) (0.6 mmol, 0.1189 g) with a molar ratio of 2 : 1 : 2 was sealed in a 25 mL Teflon-lined stainless steel Parr bomb containing deionized water (9 mL) and ethanol (9 mL). The system was heated at 100 °C for 72 h and then cooled to room temperature. Red acicular crystals of **1-Nd** were obtained (yield 51% based on Nd). Anal. calcd. for **1-Nd**, $C_{48}H_{32}Fe_2Nd_2N_6O_{14}$: C, 43.7%; H, 2.4%; O, 17.0%; N, 6.4%; found: C, 43.8%; H, 2.5%; O, 17.1%; N, 6.4%. FTIR (KBr)/cm^{-1}: 3078 w, 1625 w, 1566 s, 1481 s, 1394 s, 1361 m, 1290 m, 1188 m, 1102 m, 1026 m, 846 m, 804 m, 730 m, 506 s.

Synthesis of $[Ln_2(fcd)_3(phen)_2]{\cdot}(CH_3OH)_2$ (Ln = Sm (2-Sm), Eu (2-Eu), Gd (2-Gd), Tb (2-Tb)). The synthesis of red acicular crystals of **2-Sm** followed the same procedure as for **1-Nd** except that the molar ratio of $LnCl_3{\cdot}nH_2O$, H_2fcd and phen changed from 2 : 1 : 2 to 2 : 1 : 4, ethanol was replaced by methanol and $Nd(NO_3)_3{\cdot}6H_2O$ was replaced by $SmCl_3{\cdot}6H_2O$ (0.6 mmol, 0.2189 g; yield 52% based on Sm). Calcd. for **2-Sm**, $C_{62}H_{48}Fe_3Sm_2N_4O_{14}$: C, 48.3%; H, 3.1%; O, 14.5%; N, 3.6%; found: C, 48.3%; H, 3.2%; O, 14.6%; N, 3.6%. FTIR (KBr)/cm^{-1}: 3078 w, 1647 w, 1580 s, 1482 s, 1390 s, 1352 m, 1189 w, 1101 w, 1023 w, 844 m, 800 m, 730 m, 515 m. **2-Eu/Gd/Tb** were synthesized by following the above-stated procedure, and the details are described in the ESI.†

Synthesis of $Ln_2(fcd)_2(Hfcd)_2(phen)_2$ (Ln = La (3-La), Ce (3-Ce), Pr (3-Pr), Nd (3-Nd), Sm (3-Sm), Gd (3-Gd)). The synthesis of red acicular crystals of **3-Nd** followed the same procedure as for **1-Nd** except that $Nd(NO_3)_3{\cdot}6H_2O$ was replaced by $NdCl_3{\cdot}7H_2O$ (0.6 mmol, 0.2260 g; yield 49% based on Nd). Calcd. for **3-Nd**, $C_{72}H_{50}Fe_4Nd_2N_4O_{16}$: C, 49.7%; H, 2.9%; O, 14.7%; N, 3.2%; found: C, %; H, %; O, %; N, %. FTIR (KBr)/cm^{-1}: 3365 vw, 3121 w, 1645 w, 1575 s, 1478 s, 1389 s, 1351 s, 1187 m, 1022 m, 844 m, 799 m, 729 m, 515 m. **3-La/Ce/Pr/Sm/Gd** were synthesized by following the above-stated procedure, and the details are described in the ESI.†

Synthesis of $[Ln_2(fcd)_3(CH_3CH_2OH)_2(H_2O)_2]{\cdot}H_2O$ (Ln = La (4-La), Ce (4-Ce), Pr (4-Pr), Nd (4-Nd), Sm (4-Sm), Eu (4-Eu), Gd (4-Gd), Tb (4-Tb), Dy (4-Dy), Er (4-Er), Tm (4-Tm), Yb (4-Yb)). The synthesis of red block-like crystals of **4-Nd** followed the same procedure as for **1-Nd** except that the molar ratio of $LnCl_3{\cdot}nH_2O$, H_2fcd and phen changed from 2 : 1 : 2 to 2 : 1 : 1 and $Nd(NO_3)_3{\cdot}6H_2O$ was replaced by $NdCl_3{\cdot}7H_2O$ (0.6 mmol, 0.2260 g; yield 39% based on Nd). Calcd. for **4-Nd**, $C_{40}H_{42}Fe_3Nd_2O_{17}$: C, 38.4%; H, 3.4%; O, 21.7%; found: C, %; H, %; O, %. FTIR (KBr)/cm^{-1}: 3380 vw, 3122 w, 1645 m, 1576 m, 1479 m, 1389 s, 1351 s, 1188 w, 1023 w, 800 m, 730 m, 516 m. **4-La/Ce/Pr/Sm/Eu/Gd/Tb/Dy/Er/Tm/Yb** were synthesized by following the above-stated procedure, and the details are described in the ESI.†

Synthesis of $[Ln_4(fcd)_6(H_2O)_2]{\cdot}nCH_3CH_2OH$ (Ln = Sm (5-Sm), Eu (5-Eu) and Tb (5-Tb)). The synthesis of block-like crystals of **5-Sm** followed the same procedure as for **4-Nd** except that the temperature changed from 100 °C to 120 °C and $NdCl_3{\cdot}7H_2O$ was replaced by $SmCl_3{\cdot}6H_2O$ (0.6 mmol; 0.2189 g, yield 5% based on Sm). Calcd. for **5-Sm**, $C_{36.67}H_{28}Fe_3Sm_2O_{13.34}$: C, 38.2%; H, 2.4%; O, 18.6%; found: C, 37.9%; H, 2.5%; O, 18.9%. FTIR (KBr)/cm^{-1}: 3354 w, 1647 w, 1483 s, 1392 s, 1352 s, 1188 m, 1023 m, 844 m, 800 m, 763 m, 605 w, 514 m. **5-Eu** and **5-Tb** were synthesized by following the above-stated procedure, and the details are described in the ESI.†

Single-crystal structure determination. Single-crystal X-ray diffraction data collection for all CPs was performed with a Bruker Smart 1000 CCD area detector diffractometer with graphite-monochromatized MoKα radiation (λ = 0.71073 Å) using the ψ–ω mode at 298(2) K. The SMART software[38] was used for data collection and the SAINT software[39] for data extraction. Empirical absorption corrections were performed with the SADABS program.[40] The structures were solved by direct methods (SHELXS-2015)[41] and refined by full-matrix least-squares techniques on F^2 with anisotropic thermal parameters for all of the non-hydrogen atoms (SHELXL-2015).[41] All hydrogen atoms were located by Fourier difference synthesis and geometrical analysis. These hydrogen atoms were allowed to ride on their respective parent atoms. All structural calculations were carried out using the SHELX-2015 program package.[41] The crystal data for all CPs are listed in Tables 1 and S1.† Selected bond distances and angles for all CPs are listed in Table S2.†

Results and discussion

Synthesis

Red crystals of twenty-six CPs were synthesized by reacting H_2fcd with $LnCl_3{\cdot}nH_2O$ (Ln = La, Ce, Pr, Nd, Sm, Eu, Gd, Tb,

Table 1 Details of X-ray data collection and refinement for **1-Nd**, **2-Sm**, **3-Nd**, **4-Nd**, and **5-Sm**, which represent the different typical types of CPs reported in this study

	1-Nd	**2-Sm**	**3-Nd**	**4-Nd**	**5-Sm**
Formula	$C_{48}H_{32}Fe_2Nd_2N_6O_{14}$	$C_{62}H_{48}Fe_3Sm_2N_4O_{14}$	$C_{72}H_{50}Fe_4Nd_2N_4O_{16}$	$C_{40}H_{42}Fe_3Nd_2O_{17}$	$C_{36.67}H_{28}Fe_3Sm_2O_{13.34}$
M	1316.98	1541.29	1739.04	1250.77	1150.21
Crystal system	Monoclinic	Monoclinic	Triclinic	Monoclinic	Monoclinic
Space group	$P2_1/n$	$P2_1/n$	$P\bar{1}$	$P2/n$	$P2_1/c$
a (Å)	14.0408(13)	10.6942(9)	11.6308(11)	11.2736(12)	14.8077(12)
b (Å)	11.8581(11)	17.7327(16)	12.1047(12)	10.3725(11)	10.8766(9)
c (Å)	14.7027(14)	15.3367(14)	13.7228(13)	17.2866(17)	21.5334(18)
α (°)	90	90	94.5620(10)	90	90
β (°)	108.905(2)	108.478(2)	109.2130(10)	90.495(2)	90.5970(10)
γ (°)	90	90	117.492(2)	90	90
V (Å^3)	2315.9(4)	2758.5(4)	1555.4(3)	2021.3(4)	3467.9(5)
Z	2	2	1	2	4
μ (Mo, Kα) (mm^{-1})	2.895	2.940	2.624	3.652	4.630
Total reflections	11 612	13 725	7988	9743	17 050
Unique reflections	4070	4857	5402	3568	6119
F (000)	1292	1524	862	1232	2212
Goodness of fit on F^2	1.003	1.039	1.043	1.080	1.018
R_{int}	0.1036	0.0331	0.0274	0.0822	0.0670
R_1	0.0571	0.0308	0.0315	0.0572	0.0469
wR_2	0.1418	0.0622	0.0695	0.1319	0.1035
R_1 (all data)	0.0757	0.0517	0.0394	0.1045	0.0771
wR_2 (all data)	0.1552	0.0708	0.0725	0.1572	0.1195
Largest diff. peak and hole (e Å^{-3})	2.511, −1.853	1.182, −0.545	1.004, −0.407	3.275, −1.084	1.763, −1.068

Dy, Er, Tm, and Yb) or $Ln(NO_3)_3{\cdot}6H_2O$ (Ln = Nd) under different hydrothermal conditions, as illustrated in Scheme 1. The construction of CPs is highly influenced by experimental factors such as the coordination nature of the metal ions, the structure of the polydentate organic ligands, the metal–ligand ratio, auxiliary ligands, counterions, reaction temperature, pH and solvents. Anionic counterions play an important role in regulating and controlling the coordination mode and dimensional diversity of CPs.[26] For instance, in $Nd_2(fcd)_2(phen)_2(NO_3)_2$ (**1-Nd**) with a 0D crystal structure, two oxygen atoms from the anionic NO_3^- counterion join the Nd(III) ion in chelating mode with the third oxygen atom being terminal, which occupy the coordination sites of Nd(III) and hence prevent the structure from being extended to a higher dimension, while in $Nd_2(fcd)_2(Hfcd)_2(phen)_2$ (**3-Nd**), the absence of NO_3^- makes room for the bridging fcd^{2-} linker to extend its structure to a 1D infinite chain. The use of auxiliary ligands is also an effective method to tune the structure of the CPs, leading to tunable architectures.[27] Among the various N-donor auxiliary ligands, 1,10-phen has been widely used to build CPs, which usually contributes to the reduction of the structure dimensionality.[27,28,42] In this paper, the utilization of chelating phen indeed limits crystal structures to extend to higher dimensions, which can be illustrated by $Nd_2(fcd)_2(Hfcd)_2(phen)_2$ (**3-Nd**) with a 1D chain structure and $[Nd_2(fcd)_3(CH_3CH_2OH)_2(H_2O)_2]{\cdot}H_2O$ (**4-Nd**) with a 2D network.

Previously reported works have shown that the dimensionality of CPs can be regulated by adjusting the reaction temperature[15,20,43] since the organic ligands can adopt different conformations and coordination modes under different temperatures.[44] Furthermore, the reaction temperature can influence the coordination ability of the central metal ions.[45] Taking **4-Sm** (100 °C) and **5-Sm** (120 °C), for example, a higher temperature (120 °C) leads to more conformations and coordination modes of the fcd^{2-} ligands and a more complicated coordination environment for Sm(III) in **5-Sm** than those in **4-Sm** obtained under 100 °C. Generally, the guest solvent molecules might occupy the framework void and sometimes could

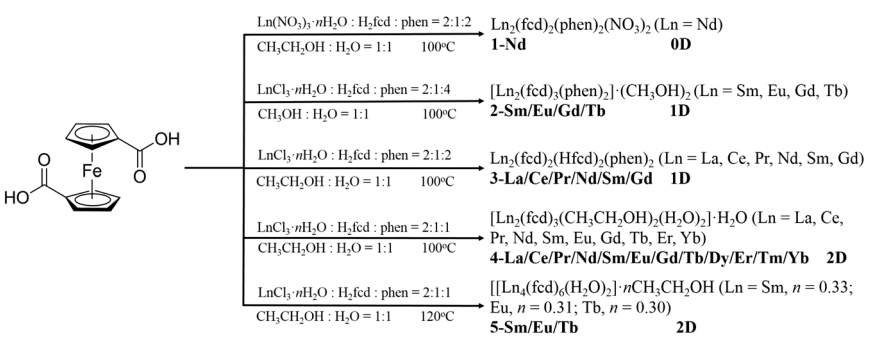

Scheme 1 Synthetic conditions of the twenty-six Ln-CPs.

even weakly coordinate to the metal centers.[46] However, solvents like water, methanol and ethanol did not affect the main structures of the twenty-six CPs in this study, as illustrated in Scheme 1.

Crystal structure description

Crystal structure of $Nd_2(fcd)_2(phen)_2(NO_3)_2$ (1-Nd). The crystal structure of **1-Nd** was composed of discrete and neutral 0D dimeric units. As illustrated in Fig. 1(a) and (b), Nd1, in a distorted tricapped trigonal prism geometry,[47] is nine-coordinated by two nitrogen atoms (N1 and N2) from one chelating phen ligand, five oxygen atoms (O1, O1A, O2A, O3 and O4A) from four carboxylate groups of two different completely deprotonated fcd^{2-} ligands, and two oxygen atoms (O5 and O6) from a NO_3^- anion. The Nd–O distances are in the range of 2.381(5)–2.685(5) Å, and the Nd–N distances are in the range of 2.602(7)–2.673(6) Å (Table S2†), which matches well with typical Nd–O and Nd–N bond lengths in previously reported counterparts.[48,49] The fcd^{2-} ligand shows a conformation between synperiplanar and synclinal-staggered with a torsion angle of *ca.* 20.2°, as exhibited in Scheme 2(a) and (b). Also, the fcd^{2-} ligand in **1-Nd** exhibited one coordination mode as shown in Scheme 3(h): one carboxylate group [O(3) and O(4)] adopts a bidentate bridging mode connecting two different Nd(III) atoms [Nd1 and Nd1A; symmetry code A: 1 −*x*, −*y*, −*z*], whereas the other carboxylate group [O1 and O2] shows a tridentate $\mu^2{:}\eta^2{:}\eta^1$-coordinating mode in which one oxygen atom (O2) is terminally bound to the neodymium atom Nd1A and the second oxygen O1 is involved in a monatomic bridge between the two Nd1 and Nd1A atoms. The coordination of NO_3^- prevents the structure from expanding into a higher-dimensional structure.

Crystal structure of $[Ln_2(fcd)_3(phen)_2]\cdot(CH_3OH)_2$ (2-Sm/Eu/Gd/Tb). **2-Sm/Eu/Gd/Tb** are isomorphous and isostructural. Hence, only the structure of **2-Sm** is described in detail. The crystal structure analysis reveals that **2-Sm** is built up of 1D infinite $[Sm_2(fcd)_3(phen)_2]$ chains and EtOH as guest molecules. As illustrated in Fig. 2(a) and (b), the distorted bicapped trigonal prismatic geometry of Sm1 is completed by two nitrogen atoms (N1 and N2) from one chelating phen ligand and six oxygen atoms (O1, O2A, O3, O4A, O5, and O6) from five carboxylate groups of three different fcd^{2-} ligands.[51]

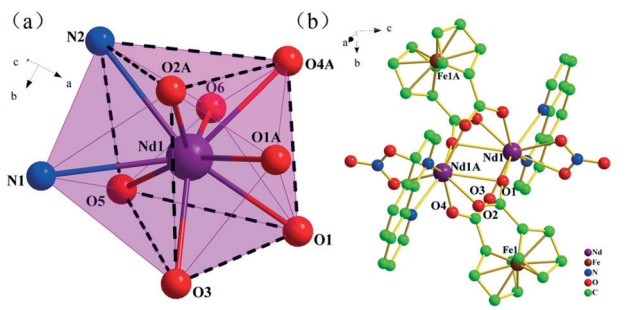

Fig. 1 (a) Highlight of the coordination polyhedron for the Nd(III) atom **1-Nd**; (b) the discrete 0D $Nd_2(fcd)_2(phen)_2(NO_3)_2$ unit in **1-Nd**.

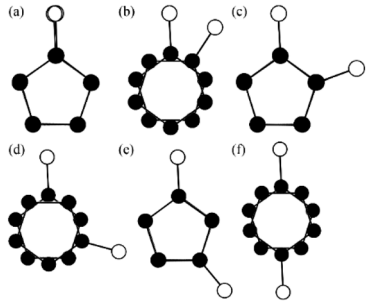

Scheme 2 Conformations of the ferrocenyl rings: (a) synperiplanar (0°); (b) synclinal-staggered (36°); (c) synclinal-eclipsed (72°); (d) anticlinal-staggered (108°); (e) anticlinal-eclipsed (144°); (f) antiperiplanar (180°).[37,50]

The Sm–O distances ranging from 2.320(3) Å to 2.473(3) Å and the Sm–N distances in the range of 2.620(4)–2.644(4) Å (Table S2†) fall into the scope of typical Sm–O and Sm–N bond lengths.[52,53] Two types of coordination modes of fcd^{2-} ligands with different conformations are present in this structure: (i) one adopts the antiperiplanar conformation with a torsion angle of *ca.* 180.0°, as illustrated in Scheme 2(f). Each carboxylate group [O5A and O6A or O5B and O6B] exhibits a bidentate chelating mode linking one Sm(III) atom, as shown in Scheme 3(f); (ii) the other fcd^{2-} ligand shows a conformation between synperiplanar (Scheme 2(a)) and synclinal-staggered (Scheme 2(b)) with a torsion angle of *ca.* 6.9°. Each carboxylate group exhibits a bidentate bridging mode linking to two different Sm(III) atoms (Scheme 3(c)). The secondary building units (SBUs) of $[Sm_2(fcd)_2(phen)_2]^{2+}$ are linked together by the bridging fcd^{2-} linker into infinite 1D $[Sm_2(fcd)_3(phen)_2]$ chains, which are packed into a two-dimensional supramolecular framework with the aid of π–π stacking interactions.

Crystal structure of $Ln_2(fcd)_2(Hfcd)_2(phen)_2$ (3-La/Ce/Pr/Nd/Sm/Gd). **3-La/Ce/Pr/Nd/Sm/Gd** are isomorphous and isostructural. The structure of **3-Nd** ($Nd_2(fcd)_2(Hfcd)_2(phen)_2$) is selected to be described in detail. The crystal structure analysis reveals that **3-Nd** is built up of 1D Nd(fcd)(Hfcd)(phen) chains. In **3-Nd**, Nd1, adopting a distorted tricapped trigonal prism geometry,[47] is coordinated by two nitrogen atoms (N1

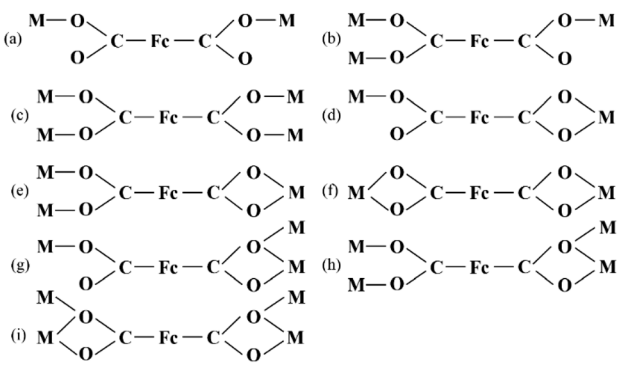

Scheme 3 Typical coordination modes for 1,1′-ferrocenedicarboxylic acid.[34]

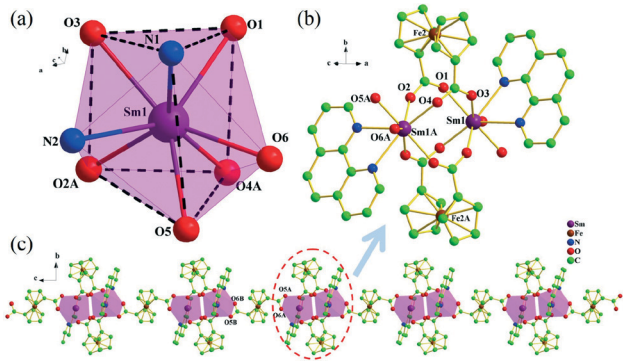

Fig. 2 (a) Highlight of the coordination polyhedron for the Sm(III) atom in **2-Sm**; (b) the secondary building unit of $[Sm_2(fcd)_2(phen)_2]^{2+}$; (c) the 1D infinite $[Sm_2(fcd)_3(phen)_2]_n$ chain in **2-Sm**.

and N2) from a chelating phen ligand and seven oxygen atoms (O1, O1A, O2A, O3, O5, O6A and O7) from six carboxylate groups of five fcd^{2-} ligands, as illustrated in Fig. 3(a) and (b). The Nd–O distances are in the range of 2.389(3)–2.827(3) Å, and the Nd–N distances are in the range of 2.656(3)–2.720(3) Å (Table S2†), which are comparable to typical Nd–O and Nd–N bond lengths in reported complexes.[48] The fcd^{2-} ligands employ two types of coordination modes with different conformations in the structure of **3-Nd**: (i) the completely deprotonated fcd^{2-} shows a conformation between anticlinal-staggered (Scheme 2(d)) and anticlinal-eclipsed (Scheme 2(e)) with a torsion angle of *ca.* 143.8°. One carboxylate group [O5A and O6A] adopts a bidentate bridging mode connecting two different neodymium atoms, and the other one adopts a monodentate bridging mode (Scheme 3(b)); (ii) the partly deprotonated $Hfcd^{-}$ shows a conformation between synclinal-staggered (Scheme 2(b)) and synclinal-eclipsed (Scheme 2(c)) with a torsion angle of *ca.* 62.8°. One carboxylate group adopts a tridentate μ^2:η^2:η^1-coordinating mode, in which one oxygen atom O2 is terminally bound to the neodymium atom Nd1A, the second oxygen O1 is involved in a monatomic bridge between the two

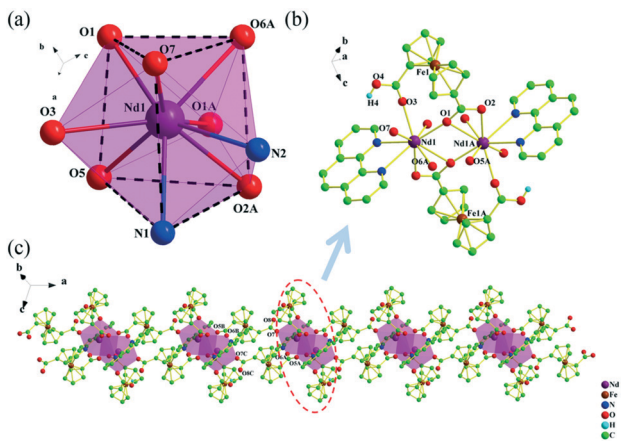

Fig. 3 (a) Highlight of the coordination polyhedron for the Nd(III) atom in **3-Nd**; (b) the secondary building unit of $[Nd_2(Hfcd)_2(phen)_2]^{4+}$; and (c) the 1D infinite $[Nd_2(Hfcd)_2(fcd)_2(phen)_2]_n$ chain in **3-Nd**.

neodymium atoms Nd1 and Nd1A, and the other one adopts a bis-monodentate bridging mode (Scheme 3(g)). The $[Sm_2(Hfcd)_2(phen)_2]^{4+}$ SBUs are linked into an infinite $[Sm_2(Hfcd)_2(fcd)_2(phen)_2]$ chain by the fcd^{2-} in an anticlinal-eclipsed conformation (as illustrated in Scheme 3(e)).

Crystal structure of $[Ln_2(fcd)_3(CH_3CH_2OH)_2(H_2O)_2]\cdot H_2O$ (4-La/Ce/Pr/Nd/Sm/Eu/Gd/Tb/Dy/Er/Tm/Yb). **4-La/Ce/Pr/Nd/Sm/Eu/Gd/Tb/Dy/Er/Tm/Yb** are isostructural. Only the structure of **4-Nd** is selected as the typical one to be described in detail. The crystal structure analysis reveals **4-Nd** as a 2D infinite $[Nd_2(fcd)_3(CH_3CH_2OH)_2(H_2O)_2]\cdot H_2O$ network structure. Two types of coordination modes of fcd^{2-} ligands with different conformations are present in this structure: (i) one ligand adopts a conformation between synclinal-staggered (Scheme 2(b)) and synclinal-eclipsed (Scheme 2(c)) with a torsion angle of *ca.* 62.5°. Each carboxylate group (O1 and O2 or O3 and O4) adopts a bidentate chelating mode, chelating one neodymium atom (Scheme 3(f)); (ii) in the other kind of ligand, fcd^{2-} exhibits an antiperiplanar conformation with a torsion angle of 180.0°, as illustrated in Scheme 2(f). Each carboxylate group adopts a bidentate bridging mode to connect two different Nd(III) atoms (Scheme 3(c)). The local environment around the Nd(III) atom is depicted in Fig. 4(a). As shown in Fig. 4(a) and (b), the distorted dodecahedral geometry of the Nd(III) ion is completed by six oxygen atoms from four bridging fcd^{2-} linkers, one oxygen atom from one coordinated ethanol molecule ligand and one oxygen atom from one coordinated water molecule.[54] It is worth noting that the carbon and hydrogen atoms (C20, H19A, H19B, H20A, H20B, and H20C) of the ethanol molecule are two disordered sites, and their corresponding site occupancy factor ratio is 0.66(2)/0.34(2). The Nd–O bond distances range from 2.406(7) to 2.892(7) Å, which are comparable to those of the counterparts reported previously.[48,49] The 2D structure is made up of the secondary building units of the $[Nd_2(fcd)_2(CH_3CH_2OH)_2(H_2O)_2]^{2+}$-linked bridging fcd^{2-} ligand. The completely deprotonated fcd^{2-} ligands, which show an antiperiplanar conformation with a torsion angle of 180.0°, play an important role in forming the 2D structure, because they not only connect each SBU through two oxygen atoms (such as O5A and O6A from one carboxylate group) but also link each chain by two carboxylate groups (such as O5, O6 and O5C, O6C). The adjacent networks are joined together into 3D sheets *via* π–π stacking interactions with a centroid–centroid distance of 3.501(7) Å.

Crystal structure of $[Ln_4(fcd)_6(H_2O)_2]\cdot n CH_3CH_2OH$ (5-Sm/Eu/Tb). **5-Sm/Eu/Tb** are isostructural, in which **5-Sm** is selected to be described in detail. The crystal structure determination reveals **5-Sm** as a 2D infinite $[Sm_4(fcd)_6(H_2O)_2]\cdot 0.33CH_3CH_2OH$ network structure. Three types of coordination modes of the fcd^{2-} ligands with different conformations are present in this structure: (i) one ligand adopts a conformation between anticlinal-eclipsed (Scheme 2(e)) and antiperiplanar (Scheme 2(f)) with a torsion angle of *ca.* 156.4°. Each carboxylate group [O5B and O6B or O7B and O8B] adopts a tridentate μ^2:η^2:η^1-coordinating mode (Scheme 3(i)).

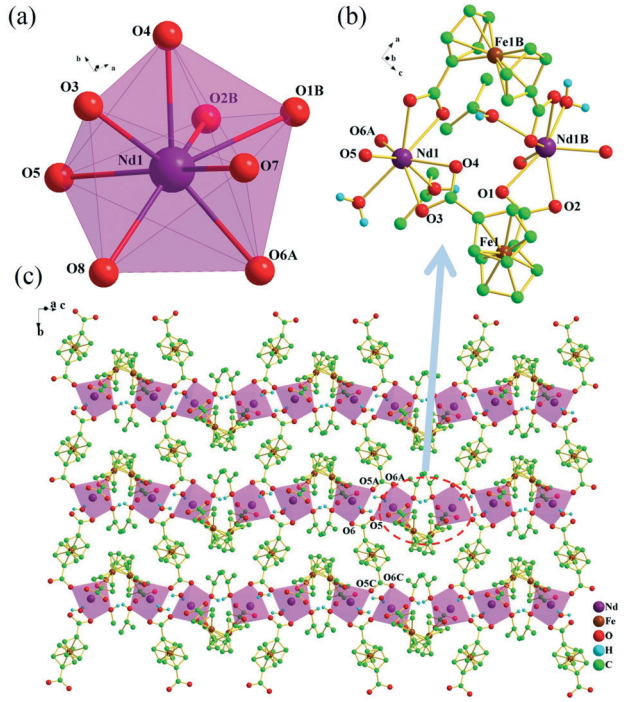

Fig. 4 (a) Highlight of the coordination polyhedron for the Nd(III) atom in **4-Nd**; (b) the secondary building unit of $[Nd_2(fcd)_2(CH_3CH_2OH)_2(H_2O)_2]^{2+}$; and (c) the 2D $[Nd_2(fcd)_3(CH_3CH_2OH)_2(H_2O)_2]_n{\cdot}nH_2O$ network of **4-Nd**.

(ii) The second ligand adopts a conformation between synclinal-staggered (Scheme 2(b)) and synclinal-eclipsed (Scheme 2(c)) with a torsion angle of *ca.* 50.0°. One carboxylate group [O3A and O4A] adopts a tridentate $\mu^2{:}\eta^2{:}\eta^1$-coordinating mode, and the other one [O1A and O2A] adopts a bidentate bridging mode connecting two different samarium atoms (Scheme 3(h)). (iii) The last one is similar to the second one, except that the torsion angle is *ca.* 19.7°. The local environment around the Sm(III) atom is depicted in Fig. 5(a) and (b). The Sm1A(III) atom, in a distorted dodecahedral geometry, is coordinated by eight oxygen atoms from six bridging fcd^{2-} linkers, as shown in Fig. 5(a) and (c). The Sm2A(III) atom, in a distorted tricapped trigonal prism geometry, is coordinated by eight oxygen atoms from four bridging fcd^{2-} linkers and one oxygen atom from one coordinated water molecule, as shown in Fig. 1(b) and (c). The Sm–O bond distances range from 2.308(5) to 2.775(6) Å, which are comparable to those of the counterparts reported previously.[52] The 2D structure of **5-Sm** can be deemed to be the assembly of $[Sm_4(fcd)_4(H_2O)_2]^{4+}$ as the secondary building units linked by the fcd^{2-} linker, as illustrated in Fig. 5(c) and (d).

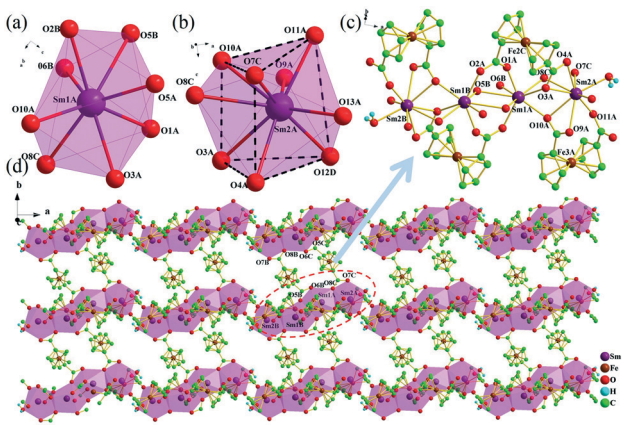

Fig. 5 (a) Highlight of the coordination polyhedron for the Sm1(III) atom in **5-Sm**; (b) highlight of the coordination polyhedron for the Sm2(III) atom in **5-Sm**; (c) the secondary building unit of $[Sm_4(fcd)_4(H_2O)_2]^{4+}$; and (d) the 2D infinite $\{[Sm_4(fcd)_6(H_2O)_2]\cdot0.33CH_3CH_2OH\}_n$ network in **5-Sm**.

Fluorescence properties

The fluorescence spectra of 1,1′-ferrocenedicarboxylic acid and the twenty-six CPs are illustrated in Fig. 6. It can be observed that all the CP powders have a wide fluorescence band centered at 389 nm, which is very similar to the emission (λ_{max} = 389 nm) observed for 1,1′-ferrocenedicarboxylic acid. Therefore, the emissions of all CPs (λ_{max} = 389 nm) can be assigned as the result of an intra-ligand transition instead of a metal-to-ligand charge transfer (MLCT) or a ligand-to-metal charge transfer (LMCT). The observed intra-ligand transition-induced fluorescence of these powders is consistent with the reported fluorescence properties of some ferrocene compounds. For example, $\{[Tb(\eta^2\text{-}O_2CFcCO_2\text{-}\eta^2)(\mu_2\text{-}\eta^2\text{-}O_2CFcCO_2\text{-}\eta^2\text{-}\mu_2)_{0.5}(H_2O)_2]\cdot2H_2O\}_n$ and $\{[Eu(\eta^2\text{-}O_2CFcCO_2\text{-}\eta^2)(\mu_2\text{-}\eta^2\text{-}O_2\text{-}CFcCO_2\text{-}\eta^2\text{-}\mu_2)_{0.5}(H_2O)_2]\cdot2H_2O\}_n$ show emission at 393 nm,[33] and $[Cd_2(\eta^2\text{-}O_2CFcCO_2)_2(2,2'\text{-bpy})_2(H_2O)_2]\cdot2H_2O$ gives an emission band at 390 nm.[34]

Magnetic properties

The interaction and possible super-exchange of the metal centers in the CPs could provide rich opportunities for tunable magnetic properties. The magnetic properties of selected CPs (**1-Nd**, **2-Sm**, **2-Eu**, **2-Tb**, **3-Ce**, **3-Pr**, **3-Nd**, **4-Ce**, **4-Pr**, **4-Nd**, **4-Sm**, **4-Eu** and **4-Tb**) were studied by both temperature-dependent susceptibility (2–300 K under an applied field of

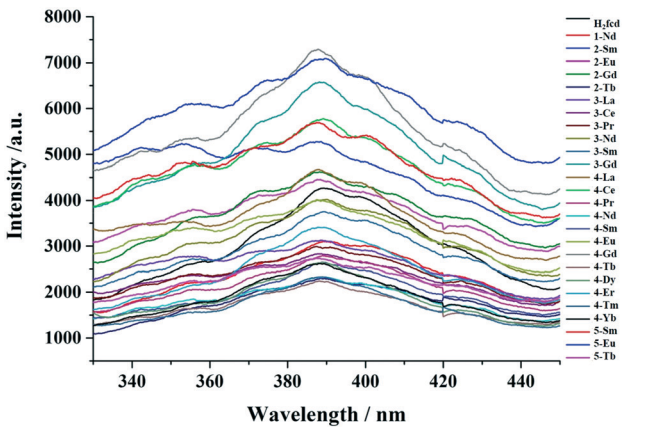

Fig. 6 Fluorescence spectra of 1,1′-ferrocenedicarboxylic acid and the twenty-six CPs in the solid state at room temperature.

1000 Oe) and field-dependent magnetization (up to 5000 Oe at 2 K) measurements (Fig. 7).

Fig. 7(a) shows the temperature-dependent $\chi_M T$ plots for Nd-containing CPs **1-Nd**, **3-Nd** and **4-Nd**. The $\chi_M T$ values at 300 K of the three CPs are 2.8–3.0 cm^3 K mol^{-1}, which are close to the value of two free Nd^{III} ions ($^4I_{9/2}$, g = 8/11).[55] A gradual decrease in their $\chi_M T$ values upon cooling can be observed for the three CPs which reaches values of 1.2–1.6 cm^3 K mol^{-1} at 2 K, which can be attributed to antiferromagnetic interactions between the spin carriers. Consistent with antiferromagnetism, the magnetization values of the Nd-containing CPs at 2 K (Fig. 7(b)) gradually increase with the field and reach 1.5 N_β, 1.7 N_β, and 1.3 N_β at 5000 Oe for **1-Nd**, **3-Nd** and **4-Nd**, respectively, which are far from the saturated value of one Nd^{III} ion.

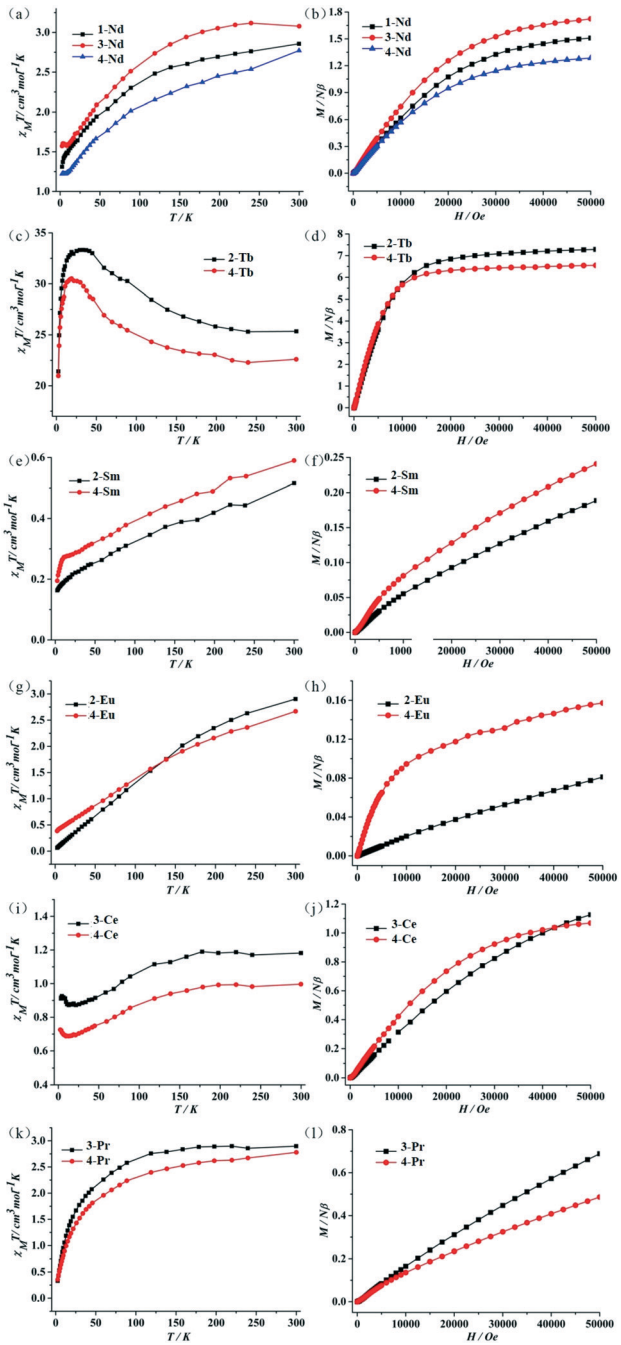

Fig. 7 Temperature-dependent $\chi_M T$ plots (calculated for two Ln^{III} ions) and field-dependent magnetization (calculated for one Ln^{III} ion) at 2 K of (a and b) Nd^{III} CPs (**1-Nd**, **3-Nd** and **4-Nd**), (c and d) Tb^{III}-containing CPs (**2-Tb** and **4-Tb**), (e and f) Sm^{III}-containing CPs (**2-Sm** and **4-Sm**), (g and h) Eu^{III}-containing CPs (**2-Eu** and **4-Eu**), (i and j) Ce^{III}-containing CPs (**3-Ce** and **4-Ce**), and (k and l) Pr^{III}-containing CPs (**3-Pr** and **4-Pr**).

For the Tb CPs **2-Tb** and **4-Tb**, the $\chi_M T$ values are 25.62 and 22.60 cm^3 K mol^{-1} at 300 K (Fig. 7(c)), which are close to the value of 23.62 cm^3 K mol^{-1} expected for two independent Tb(III) ions, considering the contribution from the 4f orbital ($^7F_6$, g = 3/2). As the temperature decreases, $\chi_M T$ increases, reaching 33.35 and 30.51 cm^3 K mol^{-1} at about 20.0 K for **2-Tb** and **4-Tb**, respectively. These magnetic behaviors indicate ferromagnetic coupling mediated by the carboxylate groups between the Tb(III) ions in **2-Tb** and **4-Tb**. However, as the temperature further decreases from 20 K to 2.0 K, an abrupt decrease in the $\chi_M T$ values of the two CPs can be observed, which might indicate a low-temperature phase transition of the onset of long-range ordering of Tb(III) within these CPs.[56] The magnetization values of **2-Tb** and **4-Tb** at 2 K (Fig. 7(d)) increase with the field and demonstrate fast saturation behavior above 15 000 Oe, which indicates the presence of ferromagnetic coupling in these CPs.[57]

The $\chi_M T$ values of the two Sm CPs **2-Sm** and **4-Sm** (Fig. 7(e)) are 0.51 and 0.59 cm^3 K mol^{-1}, respectively, which are larger than the value of 0.18 cm^3 K mol^{-1} of two independent Sm^{III} ions ($^6H_{5/2}$, g = 2/7). This might be due to the population of the first excited state $^6H_{7/2}$ at room temperature. The same situation was also found in **2-Eu** and **4-Eu** (Fig. 7(g)), in which the room temperature $\chi_M T$ values (2.90 and 2.64 cm^3 K mol^{-1}) are larger than the free-ion approximation. The decrease in the $\chi_M T$ values with decreasing temperature and slowly increasing magnetization without saturation behavior (Fig. 7(f) and (h)) suggests the onset of antiferromagnetic coupling at low temperatures.

At room temperature, the $\chi_M T$ values of two Ce-containing CPs **3-Ce** and **4-Ce** are 1.18 and 0.99 cm^3 K mol^{-1}, respectively (Fig. 7(i)), which are smaller than the theoretical value of 1.60 cm^3 K mol^{-1} for two Ce^{III} ions ($^2H_{5/2}$, g = 6/7), indicating antiferromagnetic coupling of the two CPs. A similar behavior is observed for two Pr-containing CPs (Fig. 7(k)) with $\chi_M T$ values (2.88 and 2.76 cm^3 K mol^{-1} for **3-Pr** and **4-Pr**, respectively) smaller than the theoretical value of 3.20 cm^3 K mol^{-1} for two Pr^{III} ions ($^3H_4$, g = 4/5). The magnetization values of the Pr^{III} and Ce^{III} CPs at 2 K are shown in Fig. 7(j) and (l), which increase with the field almost linearly and do not reach the saturated values, implying antiferromagnetic interaction or magnetic anisotropy.[57]

The magnetic study of the CPs indicates rich opportunities for tunable magnetic coupling between metal centers covering both antiferromagnetic and ferromagnetic behaviors of the CPs. A systematic magnetic study on the interaction and possible super-exchange of the metal centers in the CPs is currently under way.

Conclusion

In conclusion, twenty-six lanthanide coordination polymers have been synthesized under hydrothermal conditions. The conformational flexibility of the fcd ligand may lead to various assembled structures. The reaction conditions including anions, auxiliary ligands, solvent and temperature make the structures change from zero-dimensional discrete units to two-dimensional layers. The structure of **1-Nd** is a 0D cluster resulting from the occupancy of neodymium(III) coordination sites by nitrate ions. If the nitrate ions do not participate in the coordination with Ln metal ions, the structure can be extended to 1D chains, which can be found in **3-Nd**. Although the structures of the group of **2-Sm/Eu/Gd/Tb** and the group of **3-La/Ce/Pr/Nd/Sm/Gd** are 1D chains, they are different since the molar ratios of $LnCl_3{\cdot}nH_2O$, H_2fcd and phen are varied. Without the presence of chelating phen, lanthanide and fcd ligands can further form two-dimensional layers. Moreover, the temperature influences the connecting pattern between metals and ligands. All lanthanide CPs exhibit fluorescence activities resulting from intra-ligand fluorescence emissions. Also, the CPs could exhibit a variety of magnetic interactions including antiferromagnetic coupling, ferromagnetic coupling, and possible magnetic anisotropy.

Conflicts of interest

There are no conflicts to declare.

Acknowledgements

This work was supported by the National Natural Science Foundation of China (51578034), the Great Wall Scholars Training Program Project of Beijing Municipality Universities (CIT&TCD20180323), the Project of Construction of Innovation Teams and Teacher Career Development for Universities and Colleges Under Beijing Municipality (IDHT20170508), and the Beijing Talent Project (2017A38).

References

1 A. R. Millward and O. M. Yaghi, *J. Am. Chem. Soc.*, 2005, **127**, 17998–17999.
2 J. Lee, O. K. Farha, J. Roberts, K. A. Scheidt, S. T. Nguyen and J. T. Hupp, *Chem. Soc. Rev.*, 2009, **38**, 1450–1459.
3 L. E. Kreno, K. Leong, O. K. Farha, M. Allendorf, R. P. Van Duyne and J. T. Hupp, *Chem. Rev.*, 2012, **112**, 1105–1125.
4 C.-C. Wang and Y.-S. Ho, *Scientometrics*, 2016, **109**, 481–513.
5 H.-C. Zhou, J. R. Long and O. M. Yaghi, *Chem. Rev.*, 2012, **112**(2), 673–674.
6 K. Koh, A. G. Wong-Foy and A. J. Matzger, *J. Am. Chem. Soc.*, 2009, **131**, 4184–4185.
7 J.-R. Li, J. Sculley and H.-C. Zhou, *Chem. Rev.*, 2011, **112**, 869–932.
8 J.-R. Li, J. Yu, W. Lu, L.-B. Sun, J. Sculley, P. B. Balbuena and H.-C. Zhou, *Nat. Commun.*, 2013, **4**, 1538.
9 C.-C. Wang, J.-R. Li, X.-L. Lv, Y.-Q. Zhang and G. Guo, *Energy Environ. Sci.*, 2014, **7**, 2831–2867.
10 B. Chen, L. Wang, Y. Xiao, F. R. Fronczek, M. Xue, Y. Cui and G. Qian, *Angew. Chem., Int. Ed.*, 2009, **48**, 500–503.
11 P. Horcajada, T. Chalati, C. Serre, B. Gillet, C. Sebrie, T. Baati, J. F. Eubank, D. Heurtaux, P. Clayette and C. Kreuz, *Nat. Mater.*, 2010, **9**, 172–178.
12 B. Liu, H. Shioyama, H. Jiang, X. Zhang and Q. Xu, *Carbon*, 2010, **48**, 456–463.
13 N. Stock and S. Biswas, *Chem. Rev.*, 2011, **112**, 933–969.
14 F. Sun and G. Zhu, *Inorg. Chem. Commun.*, 2013, **38**, 115–118.
15 L. Luo, K. Chen, Q. Liu, Y. Lu, T.-a. Okamura, G.-C. Lv, Y. Zhao and W.-Y. Sun, *Cryst. Growth Des.*, 2013, **13**, 2312–2321.
16 S. Bauer, C. Serre, T. Devic, P. Horcajada, J. Marrot, G. Ferey and N. Stock, *Inorg. Chem.*, 2008, **47**, 7568–7576.
17 C. Volkringer, T. Loiseau, N. Guillou, G. r. Férey, M. Haouas, F. Taulelle, E. Elkaim and N. Stock, *Inorg. Chem.*, 2010, **49**, 9852–9862.
18 W.-Q. Kan, J.-F. Ma, Y.-Y. Liu, H. Wu and J. Yang, *CrystEngComm*, 2011, **13**, 7037–7043.
19 P. M. Cantos and C. L. Cahill, *Cryst. Growth Des.*, 2014, **14**, 3044–3053.
20 G.-X. Liu, H. Xu, H. Zhou, S. Nishihara and X.-M. Ren, *CrystEngComm*, 2012, **14**, 1856–1864.
21 P. Mahata, M. Prabu and S. Natarajan, *Inorg. Chem.*, 2008, **47**, 8451–8463.
22 R. Banerjee, A. Phan, B. Wang, C. Knobler, H. Furukawa, M. O'keeffe and O. M. Yaghi, *Science*, 2008, **319**, 939–943.
23 Y. Liu, Y. Qi, Y.-H. Su, F.-H. Zhao, Y.-X. Che and J.-M. Zheng, *CrystEngComm*, 2010, **12**, 3283–3290.
24 Q. Gao, Y.-B. Xie, J.-R. Li, D.-Q. Yuan, A. A. Yakovenko, J.-H. Sun and H.-C. Zhou, *Cryst. Growth Des.*, 2011, **12**, 281–288.
25 M. O. Awaleh, A. Badia and F. Brisse, *Cryst. Growth Des.*, 2006, **6**, 2674–2685.
26 H. Zhang, Z.-H. Yan, Y. Luo, X.-Y. Zheng, X.-J. Kong, L.-S. Long and L.-S. Zheng, *CrystEngComm*, 2016, **18**, 4142–4149.
27 Q. Chu, G.-X. Liu, Y.-Q. Huang, X.-F. Wang and W.-Y. Sun, *Dalton Trans.*, 2007, 4302–4311.
28 J. Gu, Z. Gao and Y. Tang, *Cryst. Growth Des.*, 2012, **12**, 3312–3323.
29 S. C. McKellar, A. J. Graham, D. R. Allan, M. I. H. Mohideen, R. E. Morris and S. A. Moggach, *Nanoscale*, 2014, **6**, 4163–4173.
30 R. Tong, Y. Zhao, L. Wang, H. Yu, F. Ren, M. Saleem and W. A. Amer, *J. Organomet. Chem.*, 2014, **755**, 16–32.
31 B. Sun, Z. Ou, D. Meng, Y. Fang, Y. Song, W. Zhu, P. V. Solntsev, V. N. Nemykin and K. M. Kadish, *Inorg. Chem.*, 2014, **53**, 8600–8609.
32 H. Jeong, D. Kim, G. Wang, S. Park, H. Lee, K. Cho, W. T. Hwang, M. H. Yoon, Y. H. Jang and H. Song, *Adv. Funct. Mater.*, 2014, **24**, 2472–2480.
33 X. Meng, G. Li, H. Hou, H. Han, Y. Fan, Y. Zhu and C. Du, *J. Organomet. Chem.*, 2003, **679**, 153–161.
34 X. Meng, H. Hou, G. Li, B. Ye, T. Ge, Y. Fan, Y. Zhu and H. Sakiyama, *J. Organomet. Chem.*, 2004, **689**, 1218–1229.

35 H. Hou, G. Li, L. Li, Y. Zhu, X. Meng and Y. Fan, *Inorg. Chem.*, 2003, **42**, 428–435.
36 J.-C. G. Bünzli, *Acc. Chem. Res.*, 2006, **39**, 53–61.
37 G. Dong, L. Yu-ting, D. Chun-ying, M. Hong and M. Qing-jin, *Inorg. Chem.*, 2003, **42**, 2519–2530.
38 S. Bruker, *AXS*, Version 5.611, Bruker AXS, Madison, WI, USA, 2000.
39 S. Bruker, *AXS*, Version 6.28, Bruker AXS, Madison, WI, USA, 2003.
40 V. SADABS, *Bruker AXS*, Madison, WI, 2000.
41 G. M. Sheldrick, *SADABS*, University of Göttingen, Göttingen, Germany, 1997.
42 L. Cuesta, E. Hevia, D. Morales, J. Pérez, L. Riera and D. Miguel, *Organometallics*, 2006, **25**, 1717–1722.
43 L.-F. Ma, L.-Y. Wang, D.-H. Lu, S. R. Batten and J.-G. Wang, *Cryst. Growth Des.*, 2009, **9**, 1741–1749.
44 J.-K. Sun, W. Li, L.-X. Cai and J. Zhang, *CrystEngComm*, 2011, **13**, 1550–1556.
45 G. Hou, L. Bi, B. Li and L. Wu, *Inorg. Chem.*, 2010, **49**, 6474–6483.
46 J.-P. Ma, Y. Yu and Y.-B. Dong, *Chem. Commun.*, 2012, **48**, 2946–2948.
47 L. Shen, L. Yang, Y. Fan, L. Wang and J. Xu, *CrystEngComm*, 2015, **17**, 9363–9369.
48 X.-J. Wang, Z.-M. Cen, Q.-L. Ni, X.-F. Jiang, H.-C. Lian, L.-C. Gui, H.-H. Zuo and Z.-Y. Wang, *Cryst. Growth Des.*, 2010, **10**, 2960–2968.
49 G.-B. Che, S.-Y. Liu, Q. Zhang, C.-B. Liu and X.-J. Zhang, *J. Solid State Chem.*, 2015, **225**, 378–382.
50 M. Kondo, Y. Hayakawa, M. Miyazawa, A. Oyama, K. Unoura, H. Kawaguchi, T. Naito, K. Maeda and F. Uchida, *Inorg. Chem.*, 2004, **43**, 5801–5803.
51 S. N. Zhao, L. J. Li, X. Z. Song, M. Zhu, Z. M. Hao, X. Meng, L. L. Wu, J. Feng, S. Y. Song and C. Wang, *Adv. Funct. Mater.*, 2015, **25**, 1463–1469.
52 G. Dong, Z. Bing-guang, D. Chun-ying, C. Xin and M. Qing-jin, *Dalton Trans.*, 2003, 282–284.
53 K. P. Carter, C. H. Zulato, E. M. Rodrigues, S. J. Pope, F. A. Sigoli and C. L. Cahill, *Dalton Trans.*, 2015, **44**, 15843–15854.
54 J. Zhu, C. Wang, F. Luan, T. Liu, P. Yan and G. Li, *Inorg. Chem.*, 2014, **53**, 8895–8901.
55 O. Kahn, *Molecular magnetism*, VCH Publishers, Inc., New York, 1993.
56 Weiwei Zheng, Pushpendra Kumar, Aaron Washington, Zhenxing Wang, Naresh S. Dalal, Geoffrey F. Strouse and Kedar Singh, *J. Am. Chem. Soc.*, 2012, **134**, 2172–2179.
57 B. Na, X. J. Zhang, W. Shi, Y. Q. Zhang, B. W. Wang, C. Gao, S. Gao and P. Cheng, *Chemistry*, 2014, **20**, 15975–1597580.

